

Effects of the constraint's curvature on structural instability: tensile buckling and multiple bifurcations

D. BIGONI^{*1}, D. MISSERONI¹, G. NOSELLI² AND D. ZACCARIA³

¹ *Department of Mechanical and Structural Engineering, University of Trento
via Mesiano 77, Trento, Italy.*

² *Department of Engineering, University of Cambridge, Trumpington Street,
Cambridge, UK.*

³ *Department of Civil and Environmental Engineering, University of Trieste
piazzale Europa 1, Trieste, Italy.*

Abstract

Bifurcation of an elastic structure crucially depends on the curvature of the constraints against which the ends of the structure are prescribed to move, an effect which deserves more attention than it has received so far. In fact, we show theoretically and we provide definitive experimental verification that an appropriate curvature of the constraint over which the end of a structure has to slide strongly affects buckling loads and can induce: (i.) tensile buckling; (ii.) decreasing- (softening), increasing- (hardening), or constant-load (null stiffness) postcritical behaviour; (iii.) multiple bifurcations, determining for instance two bifurcation loads (one tensile and one compressive) in a single-degree-of-freedom elastic system. We show how to design a constraint profile to obtain a desired postcritical behaviour and we provide the solution for the elastica constrained to slide along a circle on one end, representing the first example of an inflexional elastica developed from a buckling in tension. These results have important practical implications in the design of compliant mechanisms and may find applications in devices operating in quasi-static or dynamic conditions, even at the nanoscale.

Keywords: Constraint curvature, tensile instability, postcritical behaviour, elastica

1 Introduction

We begin with a simple example, by considering a one-degree-of-freedom elastic structure made up of a rigid rod connected with a rotational linear elastic spring on its left end and with a roller constrained to move on a circle (of radius R_c , centred on the rod's axis) on the right (Fig. 1). The structure is subject to a horizontal force, so that when this load is compressive and the circle degenerates to a line (null curvature), the structure buckles at the compressive force $F = -k/l$. Our interest is to analyze the case when the curvature of the constraint is not null, revealing that this curvature strongly affects the critical load, which results to be a *tensile*

^{*}Corresponding author: e-mail: bigoni@ing.unitn.it; phone: +39 0461 282507.

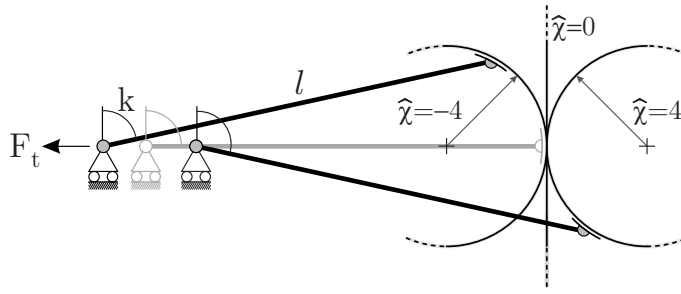


Fig. 1: A one-degree-of-freedom structure (with a rotational elastic spring at its left end) evidencing compressive or tensile buckling as a function of the curvature of the constraint (a circular profile with constant curvature, $\hat{\chi} = \pm 4$) on which the hinge on the right of the structure has to slide.

force¹ in the negative curvature case ($F_t = k/(3l)$, for $\hat{\chi} = l/R_c = -4$) and a compressive load for positive curvature ($F_c = -k/(5l)$, for $\hat{\chi} = l/R_c = 4$).

The example shows that the curvature of the constraint at the end of a structure deeply affects its critical load², but also the shape of the curve defining the constraint influences the postcritical behaviour, which displays a rising-load (hardening) behaviour in the case of null curvature and a decreasing-load (softening) behaviour for circular profiles (for instance, when $\hat{\chi} = \pm 4$, as in the structure shown in Fig. 1). Moreover, the postcritical behaviour connected to the tensile (compressive) bifurcation evidences force reversal, since the tensile (compressive) force needed to buckle the structure decreases until it vanishes and becomes compressive (tensile), during continued displacement of the structure end.

Once the lesson on the curvature and the shape of the constraint is clear, it becomes easy to play with these structural elements and discover several new effects. Some of these are listed in the following.

- A constraint profile can be designed to provide a ‘hardening’, ‘softening’ or even a ‘neutral’ (in which the displacement grows at constant load) postcritical behaviour. More in general, a formula will be given to determine the shape of the profile to obtain a desired postcritical behaviour, including situations in which the stability of the path changes during postcritical deformation.
- A negative and a positive curvature can be combined in an ‘S-shaped constraint’ (see the inset of Fig. 2) to yield a *one-degree-of-freedom structure with two buckling loads: one tensile and one compressive*.

In the case of the ‘S-shaped constraint’, imperfections suppress bifurcations and the stability of the equilibrium path strongly depends on the *sign* of the imperfection. For tensile forces, if the imperfection has a positive sign ($\phi_0 > 0$), the equilibrium path of the system becomes unstable after a peak in the load is reached, while if the sign is negative ($\phi_0 < 0$), the structure remains in a metastable equilibrium configuration which asymptotically approaches an unstable configuration (Fig. 2).

¹Tensile buckling of an elastic structure governed by the elastica, in which all elements are strictly subject to tension, has been recently discovered by Zaccaria *et al.* (2011).

²The fact that the curvature influences the critical load was observed in different terms already by Timoshenko and Gere (1936), who analyzed the case of the so-called ‘load through a fixed point’. However, they did not generalize the problem enough to discover that: tensile buckling, multiple bifurcations and inflexional tensile elastica during the postcritical behaviour can be obtained, which is the topic attacked in the present article.

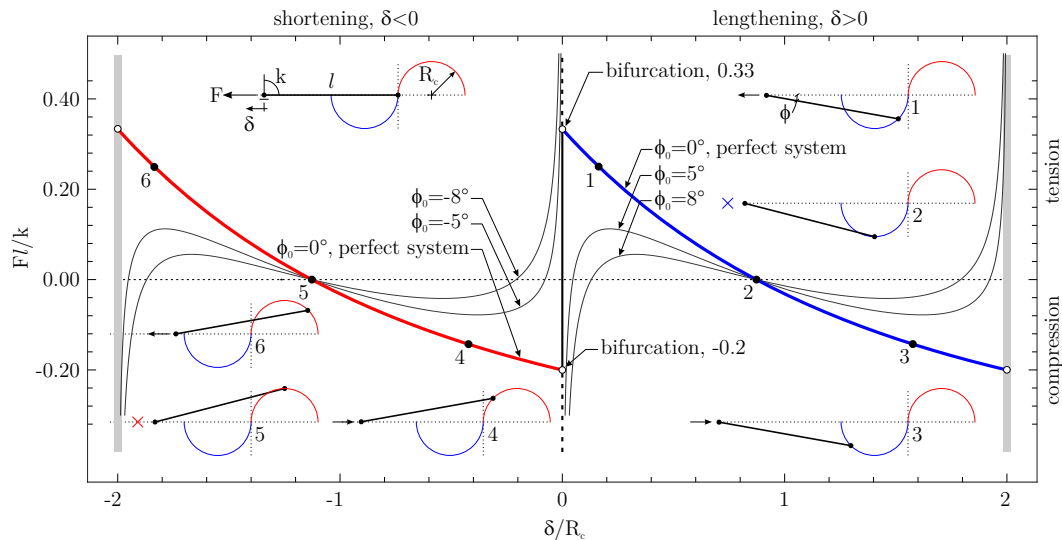


Fig. 2: The behaviour of a one-degree-of-freedom structure evidencing two buckling loads, one compressive and one tensile. These are the effect of the discontinuity in the curvature of the (piecewise circular) constraint. Note that: (i.) the two unstable postcritical branches are identical modulo a horizontal shift and that (ii.) during the postcritical behaviour there is a force reversal, with a transition from tensile (compressive) to compressive (tensile) load.

Finally, we can appreciate the role played by the curvature of a constraint in the more interesting case of a structural element governed by the elastica, a research aspect passed unnoticed until now. We show that consideration of this curvature provides a generalization of the findings by Zaccaria *et al.* (2011), so that their ‘slider’ can be seen as a special case of the curved constraint introduced in the present article and the elastica developing after a tensile buckling is of inflexional type, while that investigated by Zaccaria *et al.* (2011) is non-inflexional. We fully develop the theory of the elastica constrained to slide with a rotational spring along a circle on one of its ends and we experimentally confirm the theoretical findings with experiments designed and realized by us at the Laboratory for Physical Modeling of Structures and Photoelasticity.

The article is organized as follows. We begin presenting a generalization of the one-degree-of-freedom structure shown in Fig. 1, to highlight: (i.) the effects of the curvature of the constraint, (ii.) the multiplicity of bifurcation loads, (iii.) the behaviour of the imperfect system, and (iv.) the possibility of designing a constraint profile to obtain a given postcritical behaviour. Later we analyze a continuous system, made up of an inextensible beam governed by the Euler elastica and we solve the critical loads and the nonlinear postcritical large-deformation behaviour, through explicit integration of the elastica. We systematically complement theoretical results with experiments confirming all our findings for discrete and continuous elastic systems. A movie providing a simple illustration of the concepts exposed in this article, together with a view of experimental results, is provided in the electronic supplementary material, see also <http://ssmg.ing.unitn.it/>.

2 Effect of the constraint’s curvature on a one-degree-of-freedom elastic structure

Bifurcation load and equilibrium paths of the one-degree-of-freedom structure illustrated in Fig. 3 (where the constraint is assumed smooth and described in the x_1 - x_2 reference system as

$x_2 = l f(\psi)$, with $\psi = x_1/l \in [0, 1]$ and $f'(0) = 0$) can be calculated by considering a deformed mode defined by the rotation angle ϕ . Assuming a possible imperfection in terms of an initial inclination ϕ_0 , the elongation of the system and the potential energy are respectively

$$\delta = l [\cos \phi - \cos \phi_0 - f(\sin \phi) + f(\sin \phi_0)] \quad (1)$$

and

$$W(\phi) = \frac{1}{2}k(\phi - \phi_0)^2 - Fl [\cos \phi - \cos \phi_0 - f(\sin \phi) + f(\sin \phi_0)], \quad (2)$$

so that solutions of the equilibrium problem are governed by

$$F = -\frac{k(\phi - \phi_0)}{l[\sin \phi + \cos \phi f'(\sin \phi)]}, \quad (3)$$

where $f' = \partial f / \partial \psi$, so that the critical load for the perfect system, $\phi_0 = 0$, is

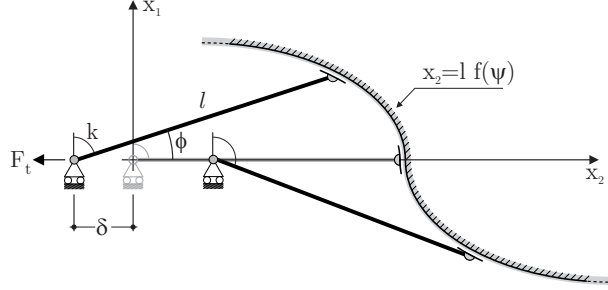


Fig. 3: A one-degree-of-freedom structure with an hinge constrained to slide along a generic smooth profile at the right end and a rotational linear-elastic spring at the left end.

$$F_{cr} = -\frac{k}{l[1 + f''(0)]}, \quad (4)$$

where, since $f'(0) = 0$, $f''(0) = \widehat{\chi}(0)$ is the signed curvature at $\phi = 0$. Stability can be judged on the basis of the sign of the second derivative of the potential energy

$$\frac{\partial^2 W(\phi)}{\partial \phi^2} = k + Fl (\cos \phi - f' \sin \phi + f'' \cos^2 \phi), \quad (5)$$

showing that the trivial configuration of the perfect system is always unstable beyond the critical load.

In the case when the profile of the constraint is a circle³ of dimensionless radius $1/|\widehat{\chi}| = 1/l|\chi|$ as in Fig. 1, the non-trivial equilibrium configurations are given by

$$F = -\frac{k(\phi - \phi_0)\sqrt{1 - \widehat{\chi}^2 \sin^2 \phi}}{l \sin \phi (\widehat{\chi} \cos \phi + \sqrt{1 - \widehat{\chi}^2 \sin^2 \phi})}, \quad (6)$$

and result to be stable when

$$1 - \widehat{\chi}^2 \sin^2 \phi - (\phi - \phi_0)(\cot \phi - \widehat{\chi} \sin \phi \sqrt{1 - \widehat{\chi}^2 \sin^2 \phi}) > 0. \quad (7)$$

Eqs. (6) and (7) have been used to solve the special case of Fig. 1 ($\widehat{\chi} = \pm 4$), with an ‘S-shaped’ constraint (so that $\widehat{\chi}$ is discontinuous at $\phi = 0$), to obtain the results plotted in Fig. 2.

³Note that in the case of a circle the dimensionless signed curvature is $\widehat{\chi} = \pm l/R_c$, with l being the length of the rigid bar and R_c the radius of the circle.

2.1 The design of the postcritical behaviour

It is important to emphasize that *the shape of the profile on which one end of the structure has to slide can be designed to obtain ‘desired postcritical behaviours’*. Let us assume that we want to obtain a certain force-displacement F/δ postcritical behaviour for the structure sketched in Fig. 3. Since

$$\delta = l \left[\sqrt{1 - \psi^2} - f(\psi) \right], \quad (8)$$

to assume a certain F/δ relation is equivalent to assume a given dependence of F on ψ ; therefore we introduce the dimensionless function

$$\beta(\psi) = \frac{l}{k} F(\delta(\psi)). \quad (9)$$

Employing Eq. (3) we obtain the condition

$$f(\psi) = \sqrt{1 - \psi^2} - \int_0^\psi \frac{\arcsin \gamma}{\beta(\gamma) \sqrt{1 - \gamma^2}} d\gamma, \quad (10)$$

satisfying $f(0) = 1$ and $f'(0) = 0$.

Three different profiles designed to obtain particular force F versus rotation ϕ postcritical behaviours (a sinusoidal, a circular and a constant) are sketched in Fig. 4. An interesting case is that of the neutral (or constant) postcritical behaviour, in which the rotation ϕ (and therefore also the displacement) can grow at constant load⁴, which can be obtained employing the constraint profile expressed as

$$f(\psi) = \sqrt{1 - \psi^2} - \frac{1}{2\beta} \left(\arcsin \psi \right)^2 \quad \text{where} \quad \beta = \frac{F_{cr} l}{k}. \quad (11)$$

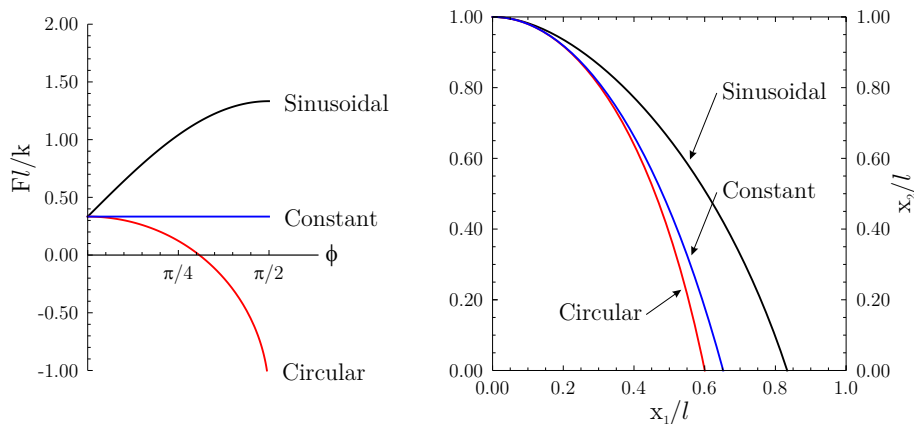


Fig. 4: Designed profiles (on the right) to obtain a given force-rotation postcritical response (on the left). The postcritical responses, given in terms of dimensionless force versus rotation of the structure are: sinusoidal, circular and constant (or ‘neutral’).

⁴A neutral postcritical behaviour has been found also by Gáspár (1984) employing a structural model completely different from that considered by us.

2.2 Experiments on one-degree-of-freedom elastic systems: multiple buckling and neutral postcritical response

The behaviours obtained employing the simple one-degree-of-freedom structures are not a mathematical curiosity, but can be realized in practice. In particular, we have realized the ‘S-shaped’ circular constraint shown in the inset of Fig. 2 and the profile illustrated in Fig. 4 (on the right, labelled ‘constant’), the latter to show a ‘neutral’ or, in other words, ‘constant-force’, response. The experimental apparatuses are shown in Fig. 5 and in Fig. 6 (the former relative to the ‘S-shaped’ semi-circular profile, the latter to the profile providing the neutral post-critical response), where the grooves have been laser cut (by HTR Laser & Water cut, BZ, Italy) in a 2 mm thick plate of AISI 304 steel and the roller has been realized with a (17 mm diameter) steel cylinder mounted with two roller bearings (SKF-61801-2Z). The rigid bar 600 mm \times 50 mm \times 20 mm have been machined from an aluminium bar and lightened with longitudinal grooves (see Appendix A), so that its final mass is 820 gr. The hinge with rotational spring has been realized with three identical rotational springs, which have been designed using equations (32) of Brown (1981) and realized in (4 mm diameter) music wire ASTM A228, see Appendix A for further details.

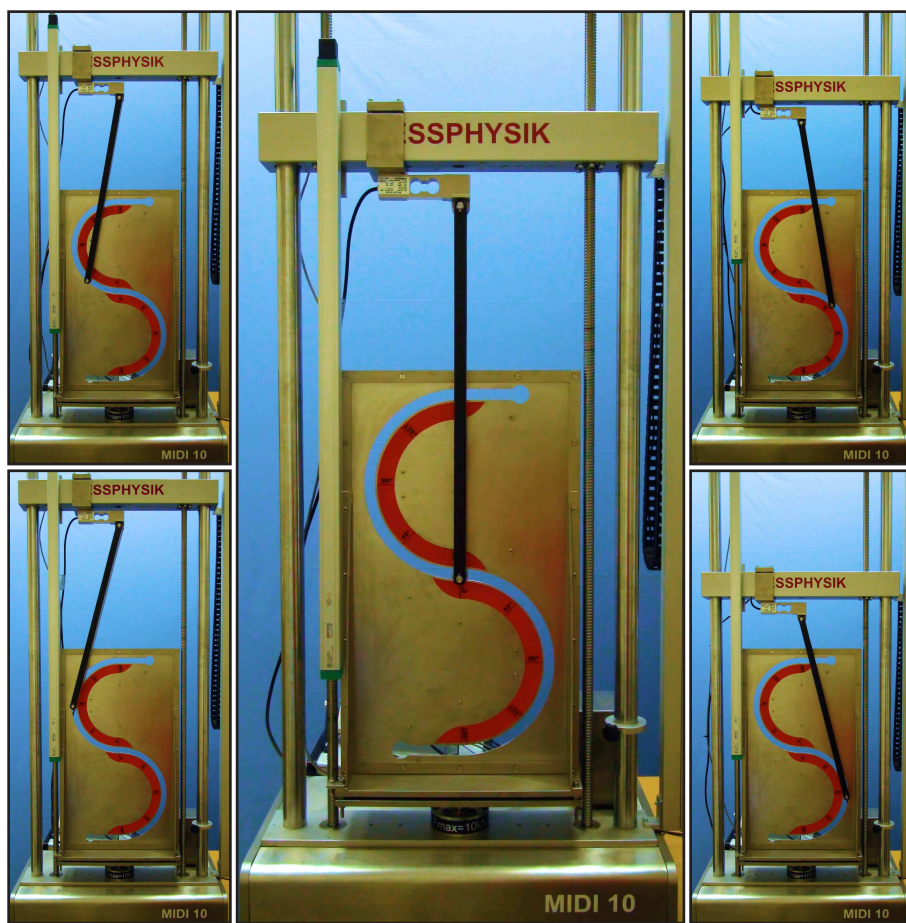


Fig. 5: Experimental set-up for the ‘S-shaped’ structure with a groove corresponding to two circles. Two photos taken during elongation (shortening) are reported on the left (on the right).

Load/displacement curves are reported in Fig. 7 for the ‘S-shaped’ circular profile and in



Fig. 6: Experimental set-up for the structure providing the neutral postcritical response. Two photos taken during elongation (shortening) are reported on the left (on the right).

Fig. 8 for the profile giving the neutral response, as obtained from experiments, and directly compared with the theoretical predictions. We note a nice agreement, with buckling detected prior to the attainment of the theoretical value, in agreement with the known effect of imperfections. Friction at the roller/profile contact has induced some irrelevant load oscillation, minimized by hand-polishing the edges of the groove and using Areo Lubricant AS 100 (from Rivolta s.p.a, Milano, Italy). We may finally comment that the experiments confirm the possibility of practically realizing mechanical systems behaving as the theoretical modelling predicts.

3 The buckling and postcritical behaviour of an elastic rod with a circular constraint on one end

We consider an *inextensible* elastic rod (of bending stiffness B and length l), with a movable clamp at one end, and having a rotational elastic spring (of stiffness k) on the other, which can slide on a circle centred on the axis of the rod, see the inset of Fig. 9. The rod is subject to an axial load F which may be tensile ($F > 0$) or compressive ($F < 0$).

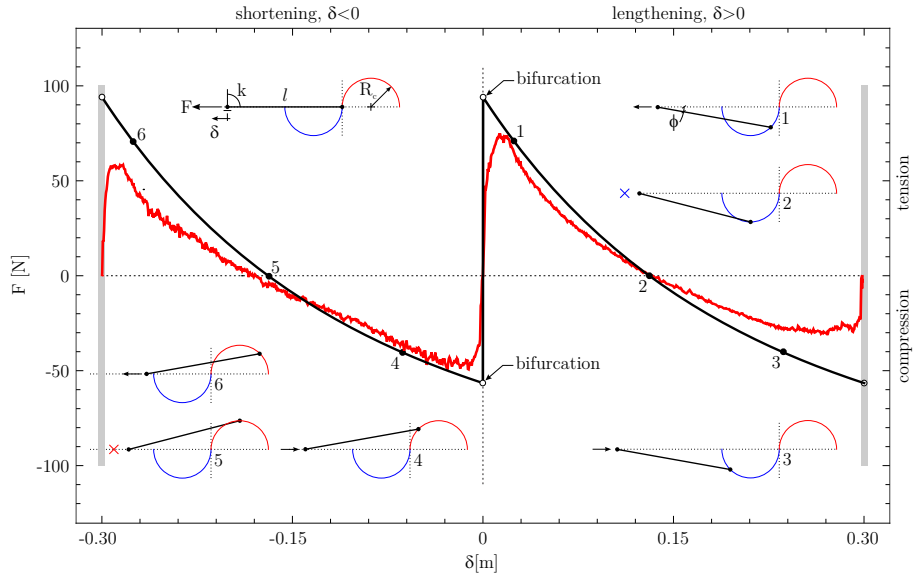


Fig. 7: Load/displacement experimental results (red line) versus theoretical prediction (black line) for a one-degree-of-freedom elastic structure having a rotational spring at one end, and a roller constrained to slide on an ‘S-shaped’, circular profile as shown in Fig. 5, together with the experimental set-up.

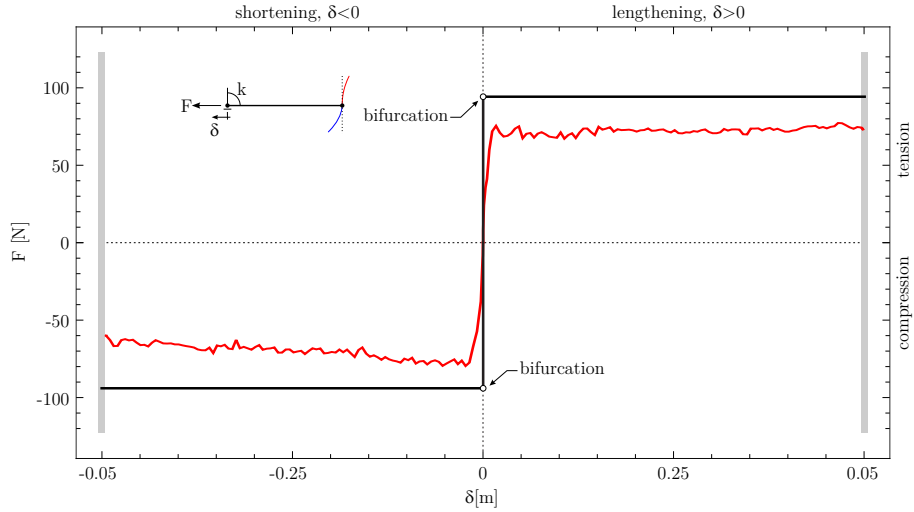


Fig. 8: Load/displacement experimental results (red line) versus theoretical prediction (black line) for a one-degree-of-freedom elastic structure designed to display a neutral postcritical behaviour. The structure has a rotational spring at one end, and a roller constrained to slide on the profile shown in Fig. 6, together with the experimental set-up.

3.1 The critical loads

The differential equilibrium equation of an elastic rod subject to an axial force F , linearized near the rectilinear configuration, is

$$\frac{d^4 v(z)}{dz^4} - \alpha^2 \operatorname{sgn}(F) \frac{d^2 v(z)}{dz^2} = 0, \quad (12)$$

where v is the transversal displacement, ‘sgn’ is defined as $\text{sgn}(\alpha) = |\alpha|/\alpha \ \forall \alpha \in \text{Re} - \{0\}$, $\text{sgn}(0) = 0$, and

$$\alpha^2 = \frac{|F|}{B}. \quad (13)$$

The general solution of Eq. (12) is

$$v(z) = \frac{C_1}{\alpha^2} \cosh(\sqrt{\text{sgn}(F)} \alpha z) + \frac{C_2}{\alpha^2} \sqrt{\text{sgn}(F)} \sinh(\sqrt{\text{sgn}(F)} \alpha z) + C_3 z + C_4, \quad (14)$$

and the boundary conditions (the third involving the rotational spring stiffness k) are:

$$\begin{aligned} v(0) = \frac{dv}{dz} \Big|_{z=0} &= 0, & (\text{null displacement and rotation at the clamped end}), \\ -\frac{\text{sgn}(F)}{\alpha^2} \frac{d^3v}{dz^3} \Big|_{z=l} &= \phi + \frac{dv}{dz} \Big|_{z=l}, & (\text{shear force on the beam at the rotational spring}), \\ -\frac{B}{k} \frac{d^2v}{dz^2} \Big|_{z=l} &= \phi + \frac{dv}{dz} \Big|_{z=l}, & (\text{moment on the beam at the rotational spring}), \end{aligned} \quad (15)$$

plus the kinematic compatibility condition defining ϕ

$$\phi = \widehat{\chi}/lv(l), \quad (16)$$

involving the signed, dimensionless curvature $\widehat{\chi} = \pm l/R_c$ of the circle.

Imposing conditions (15)–(16), the solution (14) provides the condition for the critical loads

$$\begin{aligned} & \left(\frac{1}{|\widehat{\chi}|} + \text{sgn}(\widehat{\chi}) \right) \alpha l \text{sgn}(F) \cosh(\sqrt{\text{sgn}(F)} \alpha l) - \text{sgn}(\widehat{\chi}) \sqrt{\text{sgn}(F)} \sinh(\sqrt{\text{sgn}(F)} \alpha l) \\ & + \frac{k}{B\alpha} \left[\left(\frac{1}{|\widehat{\chi}|} + \text{sgn}(\widehat{\chi}) \right) \alpha l \sqrt{\text{sgn}(F)} \sinh(\sqrt{\text{sgn}(F)} \alpha l) + \text{sgn}(\widehat{\chi}) (1 - \cosh(\sqrt{\text{sgn}(F)} \alpha l)) \right] = 0, \end{aligned} \quad (17)$$

corresponding in the two limits $k \rightarrow 0$ and $k \rightarrow \infty$ to a pinned and clamped constraint on the right end, respectively.

Buckling loads (made dimensionless through multiplication by $l^2/(\pi^2 B)$) are reported in Fig. 9 and in Tables 1 and 2, as functions of the signed radius of curvature $\widehat{\chi}$ of the constraint.

Results reported in Tables 1 and 2 (where the negative signs denote compressive loads) are given in terms of effective length factor ξ defined as

$$F_{cr} = \frac{\pi^2 B}{(\xi l)^2}. \quad (18)$$

We note from the figure and from the tables that for certain curvatures of the constraint there is one buckling load in tension, while there are always infinite bifurcations in compression (so that we can comment that the bifurcation problem remains a Sturm-Liouville problem). The results reveal the strong effect of the constraint curvature, so that for instance for $\widehat{\chi} = -1/0.2$ (for $\widehat{\chi} = -1/0.8$) there is a buckling load in tension much smaller (much higher) than that in compression, taken in absolute value. Moreover, for $\widehat{\chi} = -1/1.25$, but also for all positive curvatures $\widehat{\chi} > 0$, there is no tensile bifurcation.

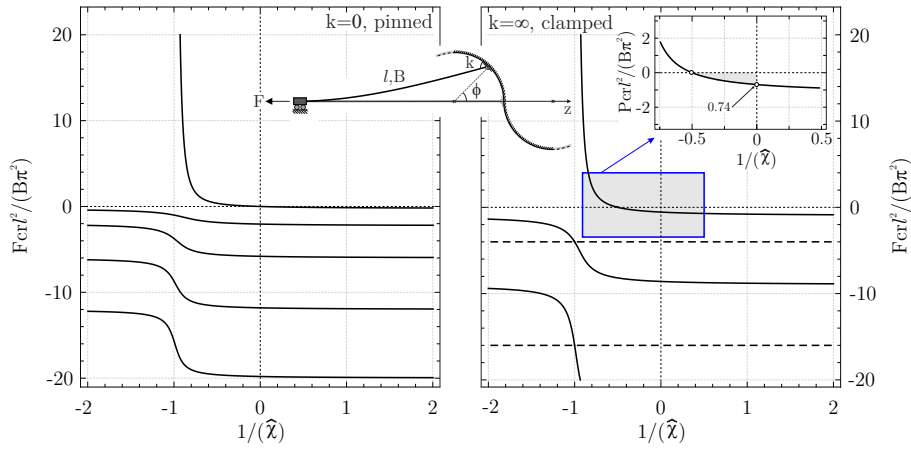


Fig. 9: Dimensionless buckling load F_{cr} (a negative sign denotes compression) of the structure sketched in the inset (clamped on the left end and sliding with a hinge, $k=0$, or guided, $k=\infty$, along a circle on the right end) as a function of the signed dimensionless curvature $\hat{\chi}$ of the circle.

$1/\hat{\chi}$	$\xi=l_0/l$	$F_{cr} l^2 / (\pi^2 B)$		$1/\hat{\chi}$	$\xi=l_0/l$	$F_{cr} l^2 / (\pi^2 B)$
-0.20	3.5373	0.0799		0.20	4.5167	-0.0490
	0.7079	-1.9955		0.40	3.4916	-0.0820
-0.40	2.0773	0.2317		0.60	3.0741	-0.1058
	0.7228	-1.9139		0.80	2.8433	-0.1237
-0.60	1.2750	0.6151		1.00	2.6954	-0.1376
	0.7529	-1.7641		1.25	2.5707	-0.1513
-0.80	0.6284	2.5326		1.50	2.4845	-0.1620
	0.8289	-1.4556		2.00	2.3722	-0.1777
-1.00	-	∞		∞	2	-0.2500
	1	-1.0000				
-1.25	1.2222	-0.6694				
-1.50	1.3726	-0.5308				
-2.00	1.8312	-0.2982				
∞	2	-0.2500				

Tab. 1: Dimensionless buckling load F_{cr} of the structure sketched in the inset (clamped on one end and with a hinge sliding along a circle on the other) as a function of the signed dimensionless curvature $\hat{\chi}$ of the circle. A negative sign denotes a compressive load.

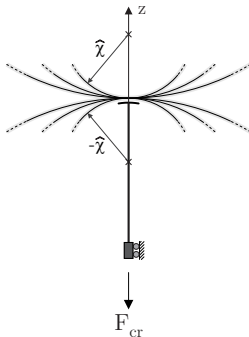
3.2 The elastica

The shape of the constraint has a strong effect on the postcritical behaviour, as will be shown below with reference to the case of the circular profile. Therefore, we derive the solution for an elastic rod clamped to the left and constrained on the right to slide with a rotational spring (of stiffness k_r) on a ‘S-shaped’ bi-circular profile, as sketched in Fig. 10, where the local reference system to be used in the analysis is also indicated.

The elastic line problem is governed by the following equations.

- i.) A condition of kinematic compatibility can be obtained by observing from Fig. 10 that the coordinates of the elastica evaluated at $s=l$, namely, $x_1(l)$ and $x_2(l)$, are related to the angle of rotation of the local reference system ϕ and to the radius R_c of the constraint via

$$[x_1(l) \mp R_c] \tan \phi - x_2(l) = 0, \quad (19)$$

$1/\hat{\chi}$	$\xi=l_0/l$	$F_{cr}l^2/(\pi^2B)$		$1/\hat{\chi}$	$\xi=l_0/l$	$F_{cr}l^2/(\pi^2B)$
-0.20	1.5372	-0.4232		0.20	1.2579	-0.6320
-0.40	2.2588	-0.1960		0.40	1.2053	-0.6884
-0.60	1.7689	0.3196		0.60	1.1704	-0.7300
	0.5	-4.0000		0.80	1.1459	-0.7616
-0.80	0.6375	2.4608		1.00	1.1274	-0.7868
	0.5	-4.0000		1.25	1.1102	-0.8114
-1.00	-	∞		1.50	1.0969	-0.8312
	0.5	-4.0000		2.00	1.0781	-0.8603
-1.25	0.6862	-2.1234		∞	1	-1.0000
-1.50	0.7742	-1.6682				
-2.00	0.8554	-1.3666				
$-\infty$	1	-1.0000				

Tab. 2: Dimensionless buckling load F_{cr} of the structure sketched in the inset (clamped on one end and guided along a circle on the other end) as a function of the signed dimensionless curvature $\hat{\chi}$ of the circle. A negative sign denotes a compressive load.

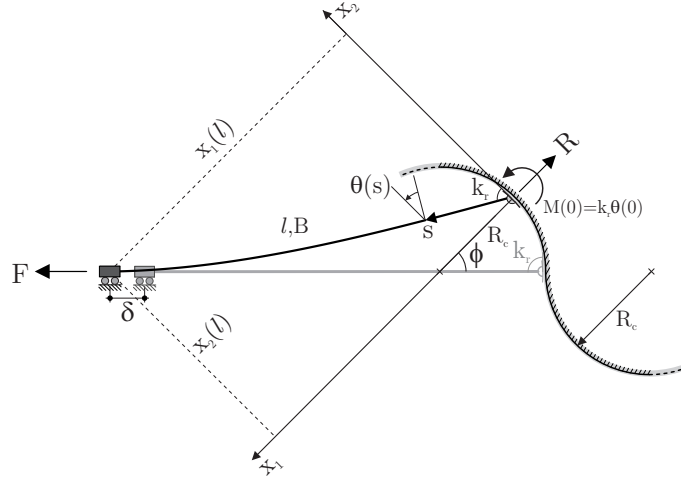


Fig. 10: The elastic line problem for a rod clamped at the left end and constrained to slide with a rotational spring (of stiffness k_r) on a circle at the right end. Note the reference system employed in the analysis.

where ϕ is assumed positive if anticlockwise; note that in Eq. (19) the sign ‘-’ (‘+’) holds for the case of the rotational spring lying on the left (right) half-circle.

- ii.) The curved constraint transmits to the rod a moment and a force pointing the centre of the circle, in other words, parallel to x_1 and assumed positive when opposite to the direction of the x_1 -axis, so that for $0 \leq \phi < \pi/2$ ($\pi/2 < \phi \leq \pi$) it corresponds to a positive tensile (negative compressive) dead force F applied to the structure defined by

$$F = R \cos \phi. \quad (20)$$

- iii.) Through introduction of the curvilinear coordinate s , the fully nonlinear equation of the elastica governing deflections of the rod is

$$\frac{d^2\theta}{ds^2} - \frac{R}{B} \sin \theta = 0, \quad (21)$$

where θ is the rotation angle (assumed positive if clockwise) of the normal at each point of the elastica, so that with the symbols introduced in Fig. 10 we find the condition

$$\theta(l) = \phi. \quad (22)$$

Integration of Eq. (21) from 0 to s , after multiplication by $d\theta/ds$, leads to

$$\left(\frac{d\theta}{ds}\right)^2 = 2\tilde{\alpha}^2 \left[\frac{2}{k^2} - 1 - \operatorname{sgn}(R) \cos \theta \right], \quad (23)$$

where

$$\tilde{\alpha}^2 = \frac{|R|}{B}, \quad k^2 = \frac{4\tilde{\alpha}^2}{[\theta(0)k_r/B]^2 + 2\tilde{\alpha}^2 [\operatorname{sgn}(R) \cos \theta(0) + 1]}, \quad (24)$$

in which the term $\theta(0)k_r$ corresponds to the moment evaluated at $s = 0$. The introduction of the change of variable

$$\beta = [\theta - H(R)\pi]/2, \quad (25)$$

where H denotes the Heaviside step function, allows to re-write Eq. (23) as

$$\left(\frac{d\beta}{ds}\right)^2 = \frac{\tilde{\alpha}^2}{k^2} (1 - k^2 \sin^2 \beta), \quad (26)$$

so that a second change of variable $u = s\tilde{\alpha}/k$ yields

$$\frac{d\beta}{du} = \pm \sqrt{1 - k^2 \sin^2 \beta}. \quad (27)$$

Restricting the treatment to the case '+', which corresponds to $\theta(0) \geq 0$, and since $\beta = \beta(0)$ at $u = 0$, Eq. (27) provides the following solution for β

$$\beta = \operatorname{am} [u + F[\beta(0), k], k], \quad (28)$$

where am and F are the Jacobi elliptic function amplitude and the incomplete elliptic integral of the first kind of modulus k , respectively (Byrd and Friedman, 1971). Keeping into account that $dx_1/ds = \cos \theta$ and $dx_2/ds = \sin \theta$, an integration provides the two coordinates x_1 and x_2 of the elastica expressed in terms of u as

$$\begin{cases} x_1 = \operatorname{sgn}(R) \frac{2}{k\tilde{\alpha}} \{(1 - k^2/2)u + E[\beta(0), k] - E[\operatorname{am}[u + F[\beta(0), k], k], k]\}, \\ x_2 = \operatorname{sgn}(R) \frac{2}{k\tilde{\alpha}} \{\operatorname{dn}[u + F[\beta(0), k], k] - \operatorname{dn}[F[\beta(0), k], k]\}, \end{cases} \quad (29)$$

in which the constants of integration are chosen so that x_1 and x_2 vanish at $s = 0$. In Eqs. (29) dn is the Jacobi elliptic function delta-amplitude of modulus k , while E is the incomplete elliptic integral of the second kind (Byrd and Friedman, 1971). Eqs. (29) generalize the expressions derived by Zaccaria *et al.* [2011, their equations (3.23) and (3.24)], which are recovered when $\theta(0) = 0$.

The horizontal displacement δ of the clamp on the left of the structure (assumed positive for a lengthening of the system) is given in the form

$$\delta = \frac{x_2}{\sin \phi} - l \mp R_c, \quad (30)$$

where, as for Eq. (19), the sign ‘-’ (‘+’) holds for the case of the rotational spring lying on the left (right) half-circle.

The axial load F can be obtained as a function of the rotation ϕ , or as a function of the end displacement δ , through the following steps.

- i.) A value for $\theta(0)$ is fixed, so that k can be expressed using Eqs. (24) as a function of R ;
- ii.) the expressions (29) for the coordinates of the elastica and Eq. (28), evaluated at $s = l$, become functions of R only;
- iii.) Eq. (22) provides ϕ , so that Eq. (19) becomes a nonlinear equation in the variable R , which can be numerically solved (we have used the function FindRoot of Mathematica[®] 6.0);
- iv.) once R is known, F , ϕ and δ can be respectively obtained from Eqs. (20), (22) and (30).

The postcritical behaviour (corresponding to the first modes branching from both tensile and compressive critical loads) of the structure is reported in Fig. 11 in terms of dimensionless axial load $4Fl^2/(B\pi^2)$ versus dimensionless displacement δ/R_c , for the particular case of a roller sliding on the profile, $k_r = 0$.

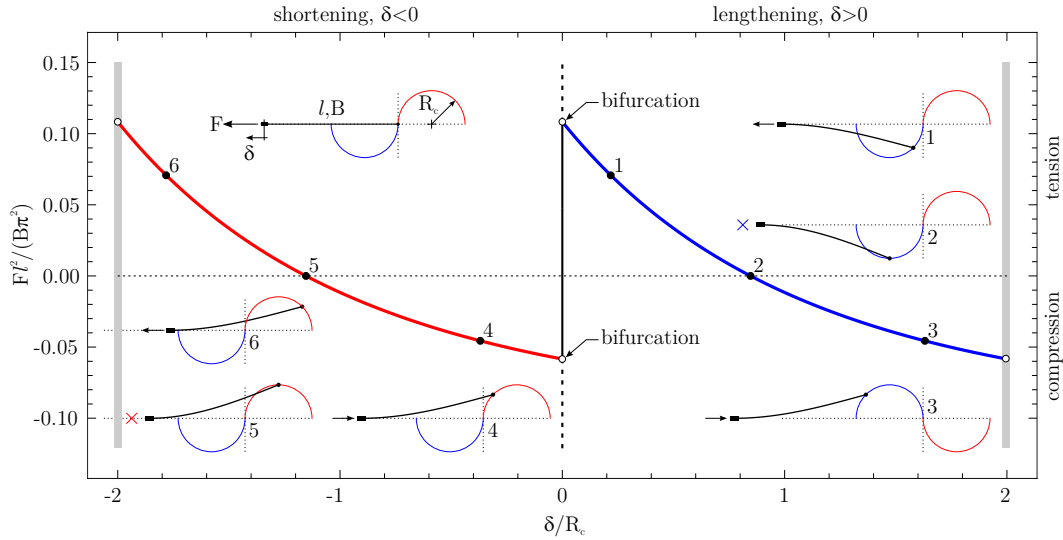


Fig. 11: The postcritical behaviour of the structure sketched in the inset (with a roller sliding on the ‘S-shaped’ profile) corresponding to the first mode under tensile and compressive loads. Dimensionless axial load F versus dimensionless end displacement.

We note that the elastica obtained in this case is *inflexional* and therefore different from that reported by Zaccaria *et al.* (2011), moreover, the postcritical behaviour is always unstable, evidencing decrease of the load with increasing edge displacement (‘softening’). Special features of the postcritical behaviour (already present in the one-degree-of-freedom system) are (i.) that there is a transition from a tensile (a compressive) to a compressive (to a tensile) elastica when the constraint reaches the points denoted with ‘2’ and ‘5’ in the graph, and that (ii.) the postcritical branches emanating from the critical loads are the same, but horizontally shifted.

3.3 Experiments on the elastica

We have tested the behaviour of an elastic rod by employing the same experimental set-up used for testing the one-degree-of-freedom structures in Sect. 2.2, but with the rigid system replaced by elastic rods realized with two $250 \text{ mm} \times 50 \text{ mm} \times 4 \text{ mm}$ C72 carbon-steel strips (Young modulus 200 GPa, mass 968 gr), see Appendix A for details. The experimental set-up with photos taken during the tests is shown in Fig. 12.

Experimental results are reported in Fig. 13 in terms of theoretical (red line) versus experimental (black line) force/end-displacement data. Moreover, the photos reported in Fig. 14,

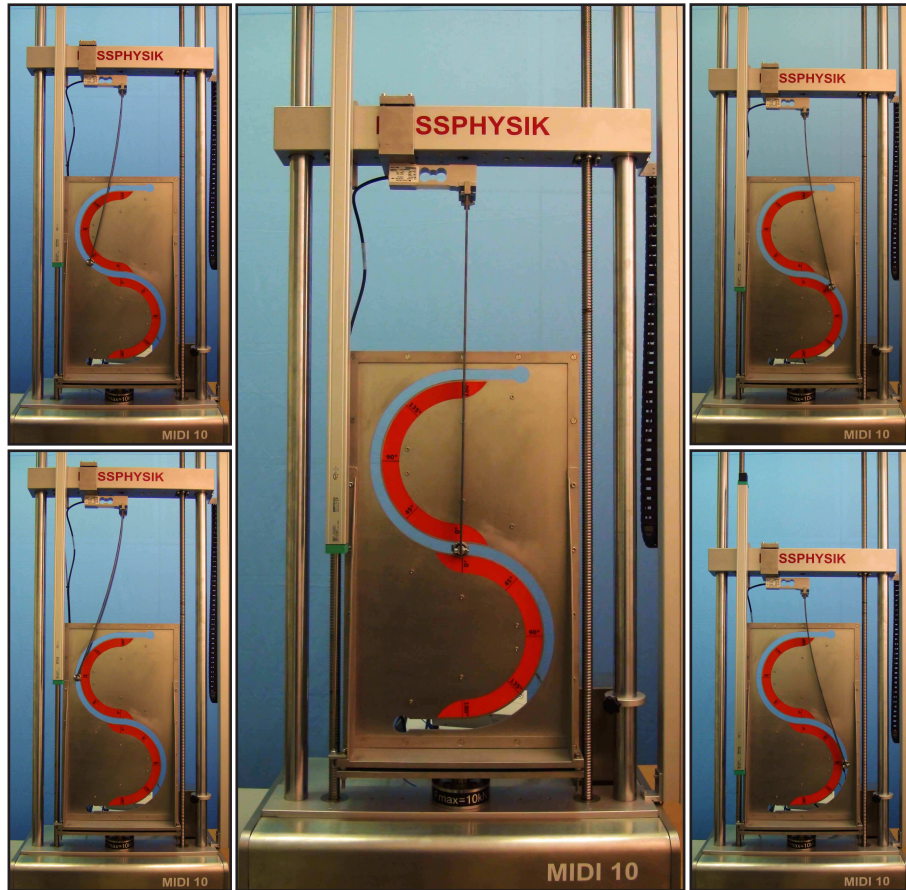


Fig. 12: Deformed shapes of the elastica during a test of a beam sliding on an ‘S-shaped’, circular profile. Two photos taken during elongation (shortening) are reported on the left (on the right).

which are details of the photos shown in Fig. 12 on the left and on the right, are compared with the theoretical shape of the elastica [shown red and obtained from Eqs. (29)] at two different end angles (45° and 90° for tension and compression).

From the figures, we can observe the following facts.

- The experiments definitely substantiate theoretical findings.
- The comparison between the deformed beam during a test and the predictions of the elastica, shown in Fig. 14, reveals a very tight agreement between theory and experiments.

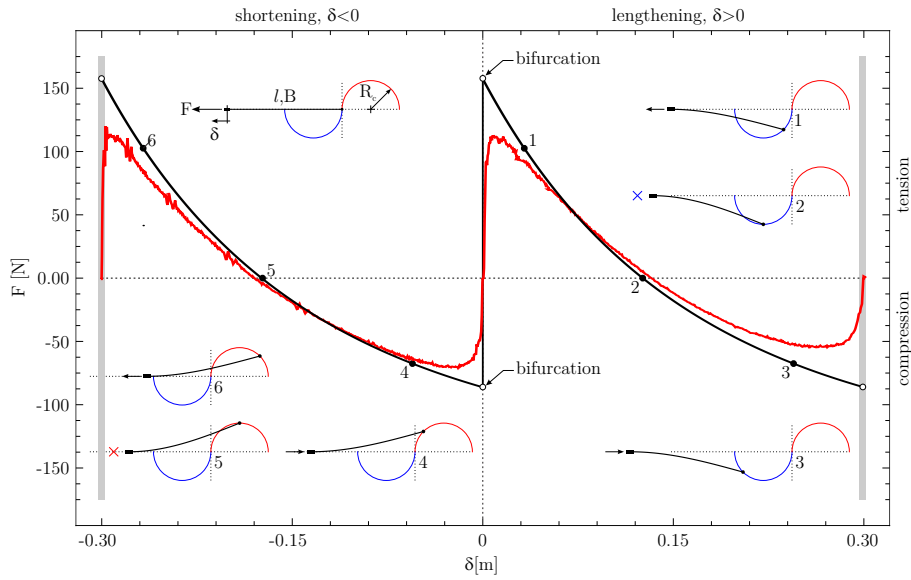


Fig. 13: Load/displacement experimental results (red line) versus theoretical prediction (black line) for a beam sliding on an ‘S-shaped’, circular profile (see the inset).

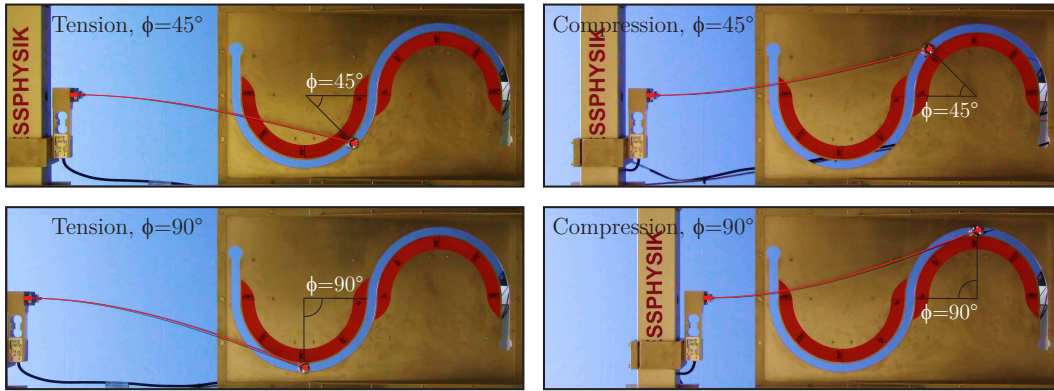


Fig. 14: Deformed shapes of the elastica (compared with the theoretical predictions reported with a red line) during the test shown in Fig. 12 of a beam with a roller sliding on an ‘S-shaped’, circular profile.

As for the one-degree-of-freedom systems, we can again conclude that the experiments confirm the possibility of practically realizing elastic systems behaving in strict agreement with theoretical predictions.

Conclusions

Effects related to the curvature and the shape of the constraint profile on which an end of a structure has to slide have been shown to be important on bifurcation and instability. In particular, we have found possibility of buckling both in tension and compression and multiple buckling loads, as for instance in the case of a one-degree-of-freedom structure evidencing two critical loads. Our experiments have confirmed that these effects can be designed to occur in real structural prototypes, so that new possibilities are opened in exploiting simple deformational

mechanisms to obtain flexible mechanical systems.

Acknowledgments

D.B. and G.N. gratefully acknowledge financial support from Italian Prin 2009 (prot. 2009XWLFKW-002); D.B. also acknowledges support from grant PIAP-GA-2011-286110.

Appendix A Details on the experimental set-up

Experiments reported in the present article have been performed at the Laboratory for Physical Modeling of Structures and Photoelasticity of the University of Trento (managed by D.B.). A Midi 10 (10 KN maximum force, from Messphysik Materials Testing) electromechanical testing machine has been employed to impose displacements (velocity 0.2 mm/s) at the ends of the structures. Loads and displacements have been measured with the loading cell and the displacement transducer mounted on the Midi 10 machine, and, independently, with a MT 1041 (0.5 kN maximum load) load cell (from Mettler-Toledo) and a potentiometric displacement transducer Gefran LTM-900-S IP65.

The rotational springs employed for the one-degree-of-freedom systems have been designed to provide a stiffness equal to 211.5 Nm by employing equations (32) of Brown (1981). After machining, the springs have been tested and found to correspond to a stiffness equal to 169.5 Nm, the value which has been used to compare experiments with theoretical results.

An IEPE accelerometer (PCB Piezotronics Inc., model 333B50) has been attached at one end of the structure to precisely detect the instant of buckling. This has been observed in all tests to correspond to an acceleration peak ranging between 0.15 and 0.2 g, while before buckling and during postcritical behaviour the acceleration did not exceed the value 0.003 g.

Data from the load cell MT 1041, the displacement transducer Gefran LTM-900-S IP65, and the accelerometer PCB 333B50 have been acquired with a system NI CompactDAQ, interfaced with Labview 8.5.1 (National Instruments), while acquisition of the data from the Midi 10 has been obtained from a Doli EDC 222 controller.

Temperature near the testing machine has been monitored with a thermocouple connected to a Xplorer GLX Pasco and has been found to lie around 22°C, without sensible oscillations during tests.

Photos have been taken with a Nikon D200 digital camera, equipped with AF Nikkor (18-35mm 1:3.5-4.5 D) lens (Nikon Corporation) and movies have been recorded during the tests with a Sony handycam (model HDR-XR550VE). The testing set-up is shown in Fig. 15. Additional material can be found at <http://ssmg.ing.unitn.it/>.

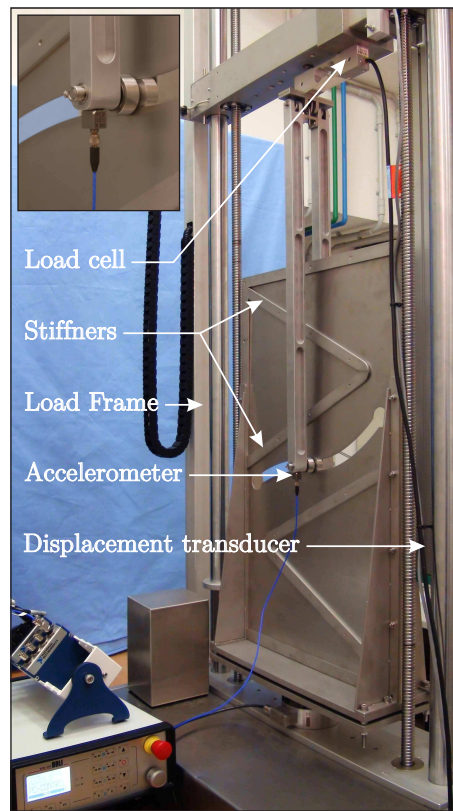


Fig. 15: The experimental set-up for the buckling tests, seen from the back.

References

- [1] Brown A.A.D. (1981) *Mechanical springs*. Oxford University Press.
- [2] Byrd, P.F and Friedman, M.D. (1971) *Handbook of elliptic integrals for engineers and scientists*. Springer-Verlag.
- [3] Gáspár, Zs. (1984) Buckling model for a degenerated case. *News Letter of the Technical University of Budapest*, 4, pp. 58.
- [4] Love, A.E.H. (1927) *A treatise on the mathematical theory of elasticity*. Cambridge University Press.
- [5] Timoshenko S.P. and Gere, J.M. (1936) *Theory of elastic stability*. McGraw-Hill.
- [6] Zaccaria, D., Bigoni, D., Noselli, G. and Misseroni, D. (2011) Structures buckling under tensile dead load. *Proc. R. Soc.A*, 2011, 467, 1686-1700.